catalysts

MDPI

Article

Impact of Black Body Material Enhanced Gas Movement on CO_2 Photocatalytic Reduction Performance

Akira Nishimura [1,*], Takaharu Kato [1], Homare Mae [1] and Eric Hu [2]

[1] Division of Mechanical Engineering, Graduate School of Engineering, Mie University, 1577 Kurimamachiya-cho, Mie 514-8507, Japan; 417122@m.mie-u.ac.jp (T.K.); 419169@m.mie-u.ac.jp (H.M.)
[2] School of Mechanical Engineering, The University of Adelaide, Adelaide 5005, Australia; eric.hu@adelaide.edu.au
* Correspondence: nisimura@mach.mie-u.ac.jp; Tel.: +81-59-231-9747

Abstract: Gas movement around and/or through the photocatalyst is thought to be an inhibition factor to promote photocatalytic CO_2 reduction performance. In this study, a hypothesis is put forward that the natural thermosiphon movement of gases around the photocatalyst can be improved by using black body material/surface. The black body material/surface that is placed underneath the photocatalyst in the reactor would be heated by absorbing light and then this heats up the gases to promote their movement around/through the photocatalyst. The aim of this study is to prove or disprove this hypothesis by conducting CO_2 reduction performance of a TiO_2 photocatalyst with NH_3 under the conditions without black body material (W/O B.B.), with one black body material (W B.B.-1), and with three black body materials (W B.B.-3). The impact of molar ratio of CO_2/NH_3 on CO_2 reduction performance is also investigated. This study revealed/proved that the hypothesis worked and that the CO_2 reduction performance is promoted more with W B.B.-3 compared to that with W B.B.-1. The maximum concentration of formed CO with W B.B.-3 is two to five times as large as that under the condition W/O B.B.

Keywords: TiO_2 photocatalyst; CO_2 reduction; black body material; infrared ray; mass transfer promotion

Citation: Nishimura, A.; Kato, T.; Mae, H.; Hu, E. Impact of Black Body Material Enhanced Gas Movement on CO_2 Photocatalytic Reduction Performance. *Catalysts* **2022**, *12*, 470. https://doi.org/10.3390/catal12050470

Academic Editor: Roberto Fiorenza

Received: 28 March 2022
Accepted: 19 April 2022
Published: 22 April 2022

1. Introduction

Many countries have set the goal to decrease CO_2 emissions by 2030 and 2050. In Japan, the prime minister has declared the aim to reduce effective CO_2 emissions to zero by 2050. However, the global average concentration of CO_2 in the atmosphere increased to 417 ppmV in December 2021, which is an increase of 77 ppmV from 1980 [1]. Therefore, it is necessary that break-through technology to reduce the amount of CO_2 is developed in the world.

This study focuses on photocatalytic CO_2 reduction. It is known that CO_2 could be converted into fuel species such as CO, CH_4, CH_3OH, etc., by a photocatalyst [2–4]. TiO_2 is a popular photocatalyst used for CO_2 reduction that performs with ultra violet (UV) [2–4]. However, pure TiO_2 can only work under UV light illumination, which accounts for only 4% of sunlight [5]. As visible light accounts for 44% of solar energy reaching the earth [5], many approaches have tried to enhance the CO_2 reduction performance of TiO_2 as a photocatalyst by expanding the wavelength of light absorbed by TiO_2. One of the popular methods is to dope metals such as Cu [6,7], Fe [8], Pd [9,10], Pt [11–13], Ag [14], alloy AuPd [15], etc. Such a metal dopant assists with absorbing the visible light. It has been reported that the optimization of a substrate for preparing TiO_2 such as graphene hollow sphere [16] and nano-sizing TiO_2 such as nano-sheet [17], nano-tube [18], and nano-wire [9] are effective for visible light absorbance.

The other approach to promote photocatalytic CO_2 reduction is the enhancement of the gas movement around the photocatalyst. Some research has reported that the membrane reactor separating the product from the reaction surface promotes photocatalytic CO_2

reduction [19–21]. According to the calculation by the author, the mass transfer time of 10^5 s to 10^{-1} s is slower than the photo reaction time of 10^{-9} s to 10^{-15} s [21]. Therefore, it is thought that the mass transfer is the inhibition factor required to speed up the photocatalytic reaction. Another reason that causes the low reforming rate is the re-organization of the products. Namely, due to the reaction surface that is covered by products, the movement of the reactants to the reaction surface is prevented and the reverse reaction, i.e., re-oxidization, which produces CO_2 from CO and CH_4, occurs. Consequently, it is desirable that the product, i.e., CO and CH_4, are removed from the reaction surface as soon as they are produced so that the reactants, i.e., CO_2 and water vapor, can continue to react on the reaction surface [21]. Fuel production can be sustained by maintaining non-equilibrium.

This study sets a hypothesis that the natural thermosiphon movement of gasses around the TiO_2 photocatalyst can be improved by using black body material, resulting in the promotion of CO_2 reduction performance. When utilizing the lamp, e.g., Xe lamp, as a light source for photocatalytic reduction, infrared (IR) light is included. As described above, TiO_2 only works under UV light illumination, meaning that IR light is not used for the photocatalytic reaction. It is thought that the black body material absorbing IR light passing through the photocatalyst can enhance the natural thermosiphon movement of gases around the TiO_2 photocatalyst. As a result, the upstream flow will be generated due to the difference in gas density caused by the temperature difference. If we utilize the sunlight for the photocatalytic reduction in the near future, it would be effective to develop the photocatalytic reactor utilizing the wavelength from UV to IR. This is a novel approach to promote photocatalytic CO_2 reduction. There is no report utilizing the natural thermosiphon movement of gasses around the TiO_2 photocatalyst brought by black body material in order to promote the CO_2 reduction performance.

The purpose of this study is to investigate the impact of the natural thermosiphon movement of gasses around the TiO_2 photocatalyst created by black body material on the CO_2 reduction performance of the TiO_2 photocatalyst. This study prepared the black body material by spraying black body spray on Cu solid discs. To investigate the effect of the natural thermosiphon movement of gasses around the TiO_2 photocatalyst created by black body material on the CO_2 reduction performance of TiO_2, this study conducted the photocatalytic CO_2 reduction under the condition without black body material (W/O B.B.), with one black body material (W B.B.-1), and with three black body materials (W B.B.-3). The TiO_2 film was prepared on the netlike glass disc by sol-gel and dip-coating methods following previous studies by the authors [22,23]. For CO_2 reduction, a reductant is important as a partner for the reaction. According to review papers [24,25], H_2O and H_2 are generally used as reductants. It is necessary to decide the optimum reductant that provides the proton (H^+) for the reduction reaction to enhance the CO_2 reduction performance. From the past studies [26–28], the reaction scheme of CO_2 reduction with H_2O can be shown as follows:

<Photocatalytic reaction>

$$TiO_2 + h\nu \rightarrow h^+ + e^- \quad (1)$$

<Oxidization reaction>

$$2H_2O + 4h^+ \rightarrow 4H^+ + O_2 \quad (2)$$

<Reduction reaction>

$$CO_2 + 2H^+ + 2e^- \rightarrow CO + H_2O \quad (3)$$

$$CO_2 + 8H^+ + 8e^- \rightarrow CH_4 + 2H_2O \quad (4)$$

Concerning the reaction scheme of CO_2 reduction reacting with H_2, this is known as follows [29]:

<Photocatalytic reaction>

$$TiO_2 + h\nu \rightarrow h^+ + e^- \quad (5)$$

<Oxidization reaction>

$$H_2 \rightarrow 2H^+ + 2e^- \quad (6)$$

<Reduction reaction>

$$CO_2 + e^- \rightarrow CO_2^- \quad (7)$$

$$CO_2^- + H^+ + e^- \rightarrow HCOO^- \quad (8)$$

$$HCOO^- + H^+ \rightarrow CO + H_2O \quad (9)$$

$$H^+ + e^- \rightarrow H \quad (10)$$

$$CO_2 + 8H^+ + 8e^- \rightarrow CH_4 + 2H_2O \quad (11)$$

Though the previous studies investigated the CO_2 reduction reacting with H_2O or H_2 [24,25], the effect of NH_3 having $3H^+$, which is superior to H_2O and H_2, on photocatalytic CO_2 reduction characteristics has not been examined yet other than the previous studies conducted by the authors using Fe [30], Cu [31,32], or Pd [32]. They have been investigated using the combination of CO_2, H_2O, and NH_3 [30–32]. However, concerning the reaction scheme to reduce CO_2 with NH_3, this is as follows [29,32]:

<Photocatalytic reaction>

$$TiO_2 + h\nu \rightarrow h^+ + e^- \quad (12)$$

<Oxidization reaction>

$$2NH_3 \rightarrow N_2 + 3H_2 \quad (13)$$

$$H_2 \rightarrow 2H^+ + 2e^- \quad (14)$$

<Reduction reaction>

$$H^+ + e^- \rightarrow H \quad (15)$$

$$CO_2 + e^- \rightarrow CO_2 \quad (16)$$

$$CO_2^- + H^+ + e^- \rightarrow HCOO^- \quad (17)$$

$$HCOO^- + H^+ \rightarrow CO + H_2O \quad (18)$$

$$CO_2 + 8H^+ + 8e^- \rightarrow CH_4 + 2H_2O \quad (19)$$

This study investigates the effect of the natural thermosiphon movement of gasses around the TiO_2 photocatalyst created by black body material on the CO_2 reduction performance of the TiO_2 photocatalyst while changing the moral ratio of CO_2 and NH_3. This study clarifies the optimum molar ratio of CO_2 and NH_3 to understand the photochemical reaction under the condition for promoting the mass transfer surrounding the photocatalyst by black body material.

2. Results and Discussion

2.1. The Characterization of TiO_2 Film

Figure 1 shows SEM (Scanning Electron Microscope) and EPMA (Electron Probe Microanalyzer) images of the TiO_2 film, which is coated on a netlike glass disc. This study obtained the black and white SEM image at 1500 times magnification, which was available for EPMA analysis. As to the EPMA images, this study indicates the concentration of each element in the observation area by diverse colors. When the amount of the element is large, light colors, e.g., white, pink, and red, are used. On the other hand, dark colors, e.g., black and blue, are used to display small amounts of elements. According to Figure 1, we can observe the TiO_2 film having a teeth-like shape coated on the netlike glass fiber. It is

thought that the temperature distribution of TiO_2 solution that adhered to the netlike glass disc was not even during the firing process because the thermal conductivity of Ti and SiO_2 at 600 K was 19.4 W/(m·K) and 1.82 W/(m·K), respectively [33]. Due to the thermal expansion and shrinkage around the netlike glass fiber, a thermal crack formed within the TiO_2 film [22]. Consequently, the TiO_2 film on the netlike glass fiber was teeth-like.

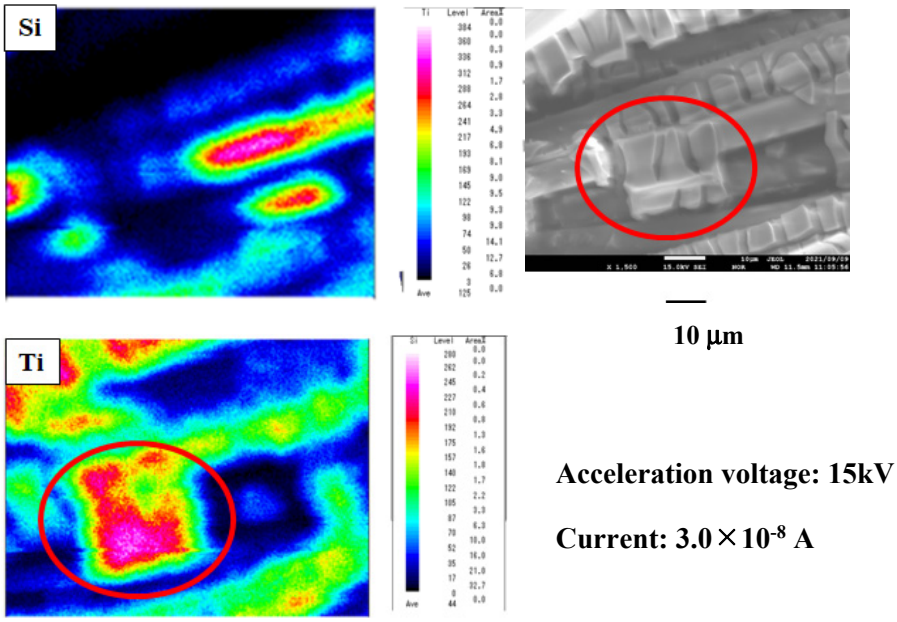

Figure 1. SEM and EPMA images of TiO_2 film, which is coated on netlike glass disc.

2.2. The CO_2 Reduction Performance with and without Black Body Material

Figure 2 shows the comparison of concentrations of formed CO and molar quantities of CO per unit weight of photocatalyst among different molar ratios with W/O B.B., W B.B.-1, and W B.B.-3, respectively. The data on the molar quantity of CO per unit weight of photocatalyst are estimated by the data on the concentration of formed CO and the weight of TiO_2 film. The weight of TiO_2 film, which was measured by electron balance, was 0.004 g. In addition, the other fuels except for CO were not detected. Regarding a blank test, this study conducted the same experiment under no Xe lamp illumination conditions as a reference case before the experiment. We detected no fuel during the blank test, as we hoped. As to the reproducibility of experiments, this study shows the data averaging three times over the experiments.

It is seen from Figure 2a,b that the highest performance was obtained in the case of CO_2:NH_3 = 1:1, where the highest concentration of formed CO is 100 ppmV and the largest molar quantity of CO per unit weight of photocatalyst is 125 μmol/g. According to the reaction scheme, as shown by Equations (12)–(19), the theoretical molar ratio to produce CO is CO_2:NH_3 = 3:2. According to Figure 2a,b, it is found that the produced CO is lower. The reason for the mismatch between the theoretical molar ratio and the optimum molar ratio obtained under this condition is due to maintaining the product near the photocatalyst surface. Therefore, this study attempts to investigate the effect of the natural thermosiphon movement of gasses around the TiO_2 photocatalyst created by black body material on CO_2 reduction performance later.

It is seen from Figure 2c,d that the highest performance was obtained in the case of CO_2:NH_3 = 3:8, where the highest concentration of formed CO is 83 ppmV and the largest molar quantity of CO per unit weight of photocatalyst is 104 μmol/g. As described above, the theoretical molar ratio to produce CO is CO_2:NH_3 = 3:2. Comparing the highest concentration of formed CO in the case of CO_2:NH_3 = 3:2 with W B.B.-1 to that with W/O B.B., the concentration of formed CO increases by 21 ppmV. Therefore, the effect of the natural thermosiphon movement of gasses around the TiO_2 photocatalyst created by black

body material on the CO_2 reduction performance is obtained. The mismatch between the theoretical molar ratio and the optimum molar ratio obtained under this condition occurred because the effect of the natural thermosiphon movement of gasses around the TiO_2 photocatalyst created by black body material might not be sufficient due to the small heat capacity of black body. Therefore, this study tries to investigate the effect of more black body materials on mass transfer surrounding the photocatalyst later.

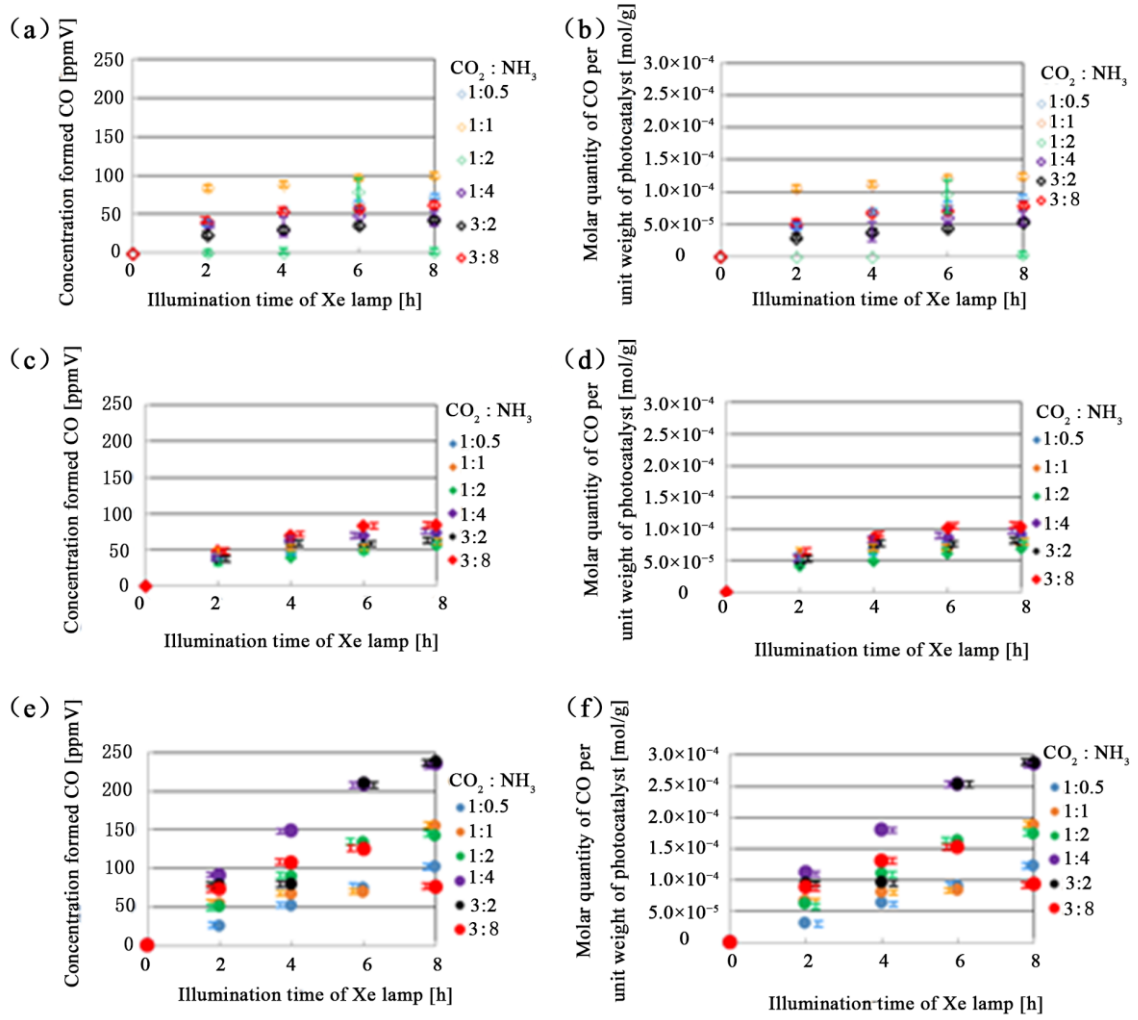

Figure 2. Comparison of concentration of formed CO among different molar ratios ((**a**,**b**): W/O B.B., (**c**,**d**): W B.B.-1, (**e**,**f**): W B.B.-3).

It is seen from Figure 2e,f that the highest performance was obtained when CO_2:NH_3 = 3:2, where the highest concentration of formed CO is 238 ppmV and the largest molar quantity of CO per unit weight of photocatalyst is 288 μmol/g. As described above, the theoretical molar ratio to produce CO is CO_2:NH_3 = 3:2, which agrees with the optimum molar ratio obtained under this condition. In addition, the highest concentration of formed CO in the case of CO_2:NH_3 = 3:2 with W B.B.-3 is higher than that with W B.B.-1 by 175 ppmV. Therefore, it is confirmed that the natural thermosiphon movement of gasses around the TiO_2 photocatalyst created by black body material could improve CO_2 reduction performance with W B.B.-3. It is thought that the mass transfer surrounding the photocatalyst is promoted by the improved natural thermosiphon movement of gasses around the TiO_2 photocatalyst created by black body material. The mechanism of these phenomena is discussed in the following section.

2.3. Relationship between Temperature of Gas in Reactor and Concentration of Formed CO

Figure 3 shows comparisons of the relationship between the temperature of gas in the reactor and the highest concentration of formed CO among different molar ratios of CO_2/NH_3 without and with black body material. The molar ratio of CO_2/NH_3 is changed by 1:0.5, 1:1, 1:2, 1:4, 3:2, and 3:8. The temperature of the gas in the reactor corresponding to the time, when the highest concentration of formed CO is obtained, is shown in these figures.

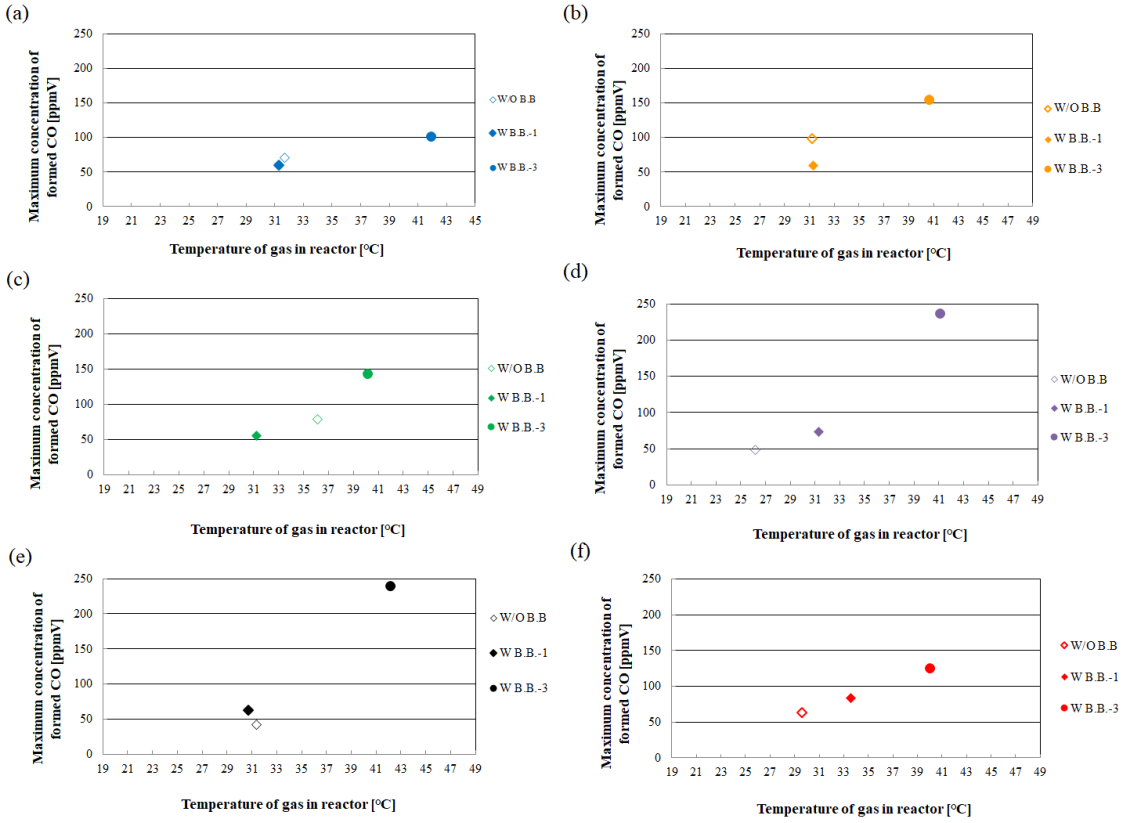

Figure 3. Relationship between temperature of gas in reactor and maximum concentration of formed CO with W/O B.B., W B.B.-1, and W B.B.-3 ((**a**): CO_2:NH_3 = 1:0.5, (**b**): CO_2:NH_3 = 1:1, (**c**): CO_2:NH_3 = 1:2, (**d**): CO_2:NH_3 = 1:4, (**e**): CO_2:NH_3 = 3:2, (**f**): CO_2:NH_3 = 3:8).

From Figure 3, it can be seen that there was almost no difference between the W B.B.-1 case and the W/O B.B. case in terms of gas temperature and the maximum concentration of formed CO. It is thought that the heat capacity of one black body material is small, resulting in the natural thermosiphon movement of gasses around the TiO_2 photocatalyst created by black body material, which is provided after heat storage by absorbing IR light, and this is not enough to heat the gas surrounding the photocatalyst. Therefore, the mass transfer surrounding the photocatalyst is not promoted, resulting in the effect of natural thermosiphon movement of gasses around the TiO_2 photocatalyst created by black body material on CO_2 reduction performance being small. On the other hand, it is found that the difference in temperature of gas in the reactor with W B.B.-3 and that with W/O B.B. is remarkable, being approximately 10 °C. Additionally, the difference in the maximum concentration of formed CO with W B.B.-3 and that with W/O B.B. is also remarkable. The maximum concentration of formed CO with W B.B.-3 is two to five times as large as that with W/O B.B. As the heat capacity of three black body materials is enough to heat the gas in the reactor, it is thought that the mass transfer surrounding the photocatalyst is promoted by the natural thermosiphon movement of gasses around the TiO_2 photocatalyst created by black body material. As a result, it is confirmed that the mass transfer promotion by black body material is effective for the improvement in CO_2 reduction performance. Moreover, it could be seen from Figure 3 that the temperature of gas in the reactor in the

case of W B.B-1 increases with the increase in the ratio of NH_3 to CO_2. The specific heat of NH_3 and CO_2 at 30 °C is 2.169 kJ/(kg·K) and 0.8518 kJ/(kg·K), respectively [33]. The specific heat of NH_3 is larger than that of CO_2. Therefore, it is thought that the mixed gas of NH_3 and CO_2 absorbs the larger heat, resulting in the temperature of the mixed gas of NH_3 and CO_2 being higher when the ratio of NH_3 to CO_2 is larger.

Figure 4 illustrates the concept of the mass transfer promotion by the natural thermosiphon movement of gasses around the TiO_2 photocatalyst created by black body material. The light illuminated from the Xe lamp penetrates through the photocatalyst because the base material is a netlike glass disc with opening space. Black body material absorbs IR light and stores the heat. After that, the natural thermosiphon movement of gasses around the TiO_2 photocatalyst created by black body material occurs when heating the gas over the TiO_2 photocatalyst. The mass transfer surrounding the photocatalyst is caused, which brings the promotion of photocatalytic CO_2 reduction. The heat capacity of Cu solid disc used for black body material is 0.189 J/K per one disc at 30 °C [33]. Therefore, the heat capacity of three Cu discs is 0.567 J/K at 30 °C. On the other hand, the volume of gas in the reactor is 1.25×10^5 mm^3. When the reactor is filled with the mixed gas of CO_2 and NH_3, whose molar ratio is 3:2, the density of mixed gas is 1.346 kg/m^3 at 30 °C [33]. The specific heat of CO_2 and NH_3 at 30 °C is 0.8546 kJ/(kg·K) and 2.171 kJ/(kg·K), respectively [33]. Considering the volume of gas in the reactor, the density, and the specific heat of mixed gas, the heat capacity of the mixed gas of CO_2 and NH_3, whose molar ratio is 3:2, is 0.402 J/K at 30 °C. Comparing the heat capacity of the mixed gas of CO_2 and NH_3 with the heat capacity of one Cu solid disc, the heat capacity of one Cu solid disc is very small. Therefore, the mixed gas of CO_2 and NH_3 is not heated well as the thermosiphon movement of gasses around the TiO_2 photocatalyst is weak. On the other hand, comparing the heat capacity of the mixed gas of CO_2 and NH_3 with the heat capacity of three Cu solid discs, the heat capacity of three Cu discs matches the heat capacity of the mixed gas of CO_2 and NH_3. It is thought that three black body materials can absorb the heat from IR light to obtain the strong natural thermosiphon movement of gasses around the TiO_2 photocatalyst. As shown in the image illustrated in Figure 4, the black body material absorbs IR light and the heat is transferred to the photocatalyst by thermal conduction. Then, the temperature of the photocatalyst rises. When one black body material is used, the temperature rise of the photocatalyst is small, resulting in the natural thermosiphon movement of gasses around the TiO_2 photocatalyst due to radiation heat being weak. On the other hand, the temperature rise of the photocatalyst is large when three black body materials are used, resulting in the natural thermosiphon movement of gasses around the TiO_2 photocatalyst due to radiation heat being strong. Therefore, it is revealed that three black body materials are needed to heat up the mixed gas of CO_2 and NH_3.

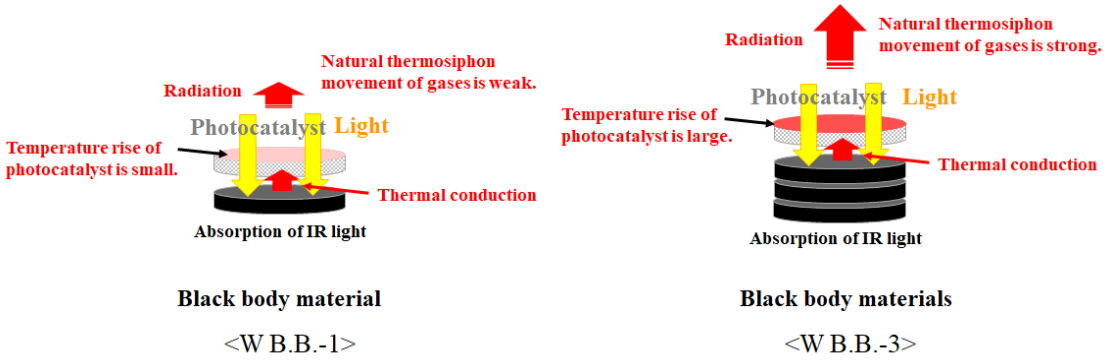

Figure 4. Concept of mass transfer promotion by natural thermosiphon movement of gasses around TiO_2 photocatalyst created by black body material.

According to the literature surveyed by this study, a product yield such as CH_4 by CO_2 reduction using Ru/TiO_2 is not changed below 100 °C [34]. Another study has reported that a product yield such as CH_4 by CO_2 reduction using montmorillonite-modified TiO_2

nanocomposites at 100 °C is eight times as large as that at 50 °C [35]. On the other hand, a product yield such as CO by CO_2 reduction using Ag-modified $CaTiO_3$ at 33 °C is lower than that at 25 °C by 15 μmol/h [36]. This study has conducted the CO_2 reduction experiment using TiO_2 within the temperature range of 26 °C to 42 °C. Therefore, this study believes the effect of the increase in temperature of the gas in the reactor on the increase in the rate of CO formation is small. In addition, the mass transfer time of 10^5 to 10^{-1} s is slower than the photo reaction time of 10^{-9} to 10^{-15} s [21], resulting in the improvement of mass transfer being more effective to promote the rate of CO formation.

To investigate the effect of black body materials prepared by this study, this study compared the thermal properties of carbon and black phosphorus with the black body material prepared. The emissivity of carbon and black body phosphorus is 0.9 and 0.95 [37], respectively. In addition, the specific heat of carbon and black phosphorus is 0.691 kJ/(kg·K) [38] and 0.67 kJ/(kg·K) [39], respectively. As described above, the heat capacity of Cu solid disc used for black material is 0.189 kJ/K per one disc when the volume of Cu solid is 5.495×10^{-8} m^3 and the density of Cu is 8879 kg/m^3. If the same volume of carbon is used, the heat capacity of carbon and black phosphorus per one disc is 0.083 kJ/K where the density of carbon is 2200 kg/m^3 [38] and 0.081 kJ/K where the density of black phosphorus is 2200 kg/m^3 [39], respectively. As the emissivity of black body material prepared by this study is 0.94, which is approximately the same as the emissivity of carbon and black phosphorus as described above, this study assumed that the radiation heat from carbon and black phosphorus is the same as that from the black body material prepared by this study. As the heat capacity of the mixed gas of CO_2 and NH_3, whose molar ratio is 3:2, is 0.402 J/K, the five discs are needed for carbon and black phosphorus to heat the gas for obtaining the mass transfer promotion by the natural thermosiphon movement of gasses.

This study believes that it is necessary to design the reactor while considering the heat balance for improving the CO_2 reduction performance of the photocatalyst in the near future. In addition, it is another challenge to combine the photocatalyst absorbing visible light with the mass transfer promotion by the natural thermosiphon movement of gasses around the photocatalyst created by black body material.

3. Experiments

3.1. The Preparation Procedure of TiO_2 Film

This study prepared TiO_2 film by sol-gel and dip-coating processes [23,31]. $[(CH_3)_2CHO]_4Ti$ (purity of 95 wt%, produced by Nacalai Tesque Co., Kyoto, Japan) of 0.3 mol, anhydrous C_2H_5OH (purity of 99.5 wt%, produced by Nacalai Tesque Co., Kyoto, Japan) of 2.4 mol, distilled water of 0.3 mol, and HCl (purity of 35 wt%, produced by Nacalai Tesque Co., Kyoto, Japan) of 0.07 mol were mixed for preparing the TiO_2 sol solution. This study coated the TiO_2 film on a netlike glass fiber (SILLIFGLASS U, produced by Nihonmuki Co., Tokyo, Japan) by sol-gel and dip-coating processes. The glass fiber, with a diameter of about 10 μm, weaved as a net, was collected to be a diameter of approximately 1 mm. The porous diameter of glass fiber and the specific surface area were about 1 nm and 400 m^2/g, respectively, from the specification of netlike glass fiber. The netlike glass fiber was composed of SiO_2 of 96 wt%. The opening space of the netlike glass fiber was approximately 2 mm × 2 mm. As the netlike glass fiber has porous characteristics, the netlike glass fiber can capture the TiO_2 film easily during sol-gel and dip-coating processes. Additionally, we can expect that CO_2 is more easily absorbed by the prepared photocatalyst due to the porous characteristics of the netlike glass fiber. This study cut the netlike glass fiber to be disc form with a diameter of 50 mm and thickness of 1 mm. This study immersed the netlike glass disc into TiO_2 sol solution while controlling the speed at 1.5 mm/s and drew it up while controlling the fixed speed at 0.22 mm/s. After that, this study dried it out and fired under a controlled firing temperature (*FT*) and firing duration time (*FD*) to fasten the TiO_2 film to the base material. This study set *FT* and *FD* at 623 K and 180 s, respectively.

3.2. The Preparation Procedure of Black Body Material

This study prepared black body material by spraying the black body spray (TA410KS, produced by ICHINEN TASCO Corp., Osaka, Japan) on both surfaces of the Cu disc. The emissivity of black body spray was 0.94. The Cu solid disc with a diameter of 50 mm and thickness of 1.4 mm was adopted as the base material for spraying black body spray. The Cu solid disc had a diameter of 50 mm equal to the inside diameter of the reactor, as explained below. The emissivity of the polished surface of Cu was 0.01 [33]. The used Cu solid disc had a purity of 99.90% [35]. The specific heat, thermal conductivity, and thermal diffusivity of Cu at 30 °C were 0.386 kJ/(kg·K), 398 W/(M·K), and 117 mm^2/s, respectively [33]. Figure 5 shows the black body material prepared by this study and the Cu solid disc before spraying black body spray.

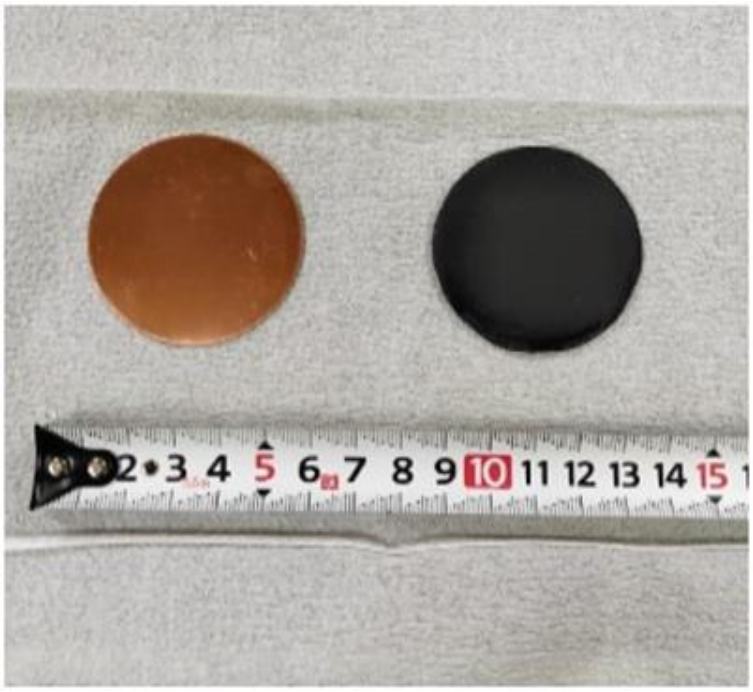

Figure 5. Photo of black body material prepared by this study and Cu solid disc before spraying black body spray.

3.3. The Characterization Procedure of TiO_2 Film

This study evaluated the characteristics of the external and crystal structure of TiO_2 film prepared above by SEM (JXA-8530F, produced by JEOL Lt., Tokyo, Japan) and EPMA (JXA-8530F, produced by JEOL Ltd., Tokyo, Japan) [23,31]. These procedures use electrons to analyze characterization, resulting in the sample conducting electricity. As the netlike glass disc used for the base material to coat TiO_2 film cannot conduct electricity, the vaporized Pt was deposited by the Pt coating device (JEC-1600, produced by JEOL Ltd., Tokyo, Japan) on the surface of the TiO_2 film before analyzing its characterization. The thickness of the deposited Pt was 15 nm. The electrons were emitted from the electrode to the sample, setting the acceleration voltage and current of 15 kV and 3.0×10^{-8} A, respectively, in order to analyze the external structure of the TiO_2 film using SEM. After the character X-ray was analyzed using EPMA at the same time, the amount of chemical element was clarified referring to the relation between character X-ray energy and atomic number. SEM and EPMA had the space resolution of 10 mm. The EPMA analysis can support clarifying the structure of the prepared TiO_2 photocatalyst.

3.4. The Experimental Procedure of CO_2 Reduction

Figure 6 illustrates the experimental apparatus where the reactor consists of a stainless tube with a scale of 100 mm (*H.*) × 50 mm (*I.D.*), the TiO_2 film is coated on a netlike glass disc with a scale of 50 mm (*D.*) × 1 mm (*t.*), positioned on the Teflon cylinder with a scale of 50 mm (*H.*) × 50 mm (*D.*), and also consisting of a quartz glass disc with a scale of 84 mm (*D.*) × 10 mm (*t.*), a 150 W Xe lamp (L2175, produced by Hamamatsu Photonics K. K.), mass flow controller, CO_2 gas cylinder (purity of 99.995 vol%), and NH_3 gas cylinder (purity of 99.99 vol%). The reactor size for charging CO_2 was 1.25×10^{-4} m^3. The light of the Xe lamp positioned on the stainless tube was illuminated toward TiO_2 film. The black body material was located under the TiO_2 film coated on a netlike glass disc. As the netlike glass disc had the aperture area of the net, which is 4 mm^2 for each, the light can reach the black body material. The mean light intensity of light illuminated from the Xe lamp was 67.6 mW/cm^2.

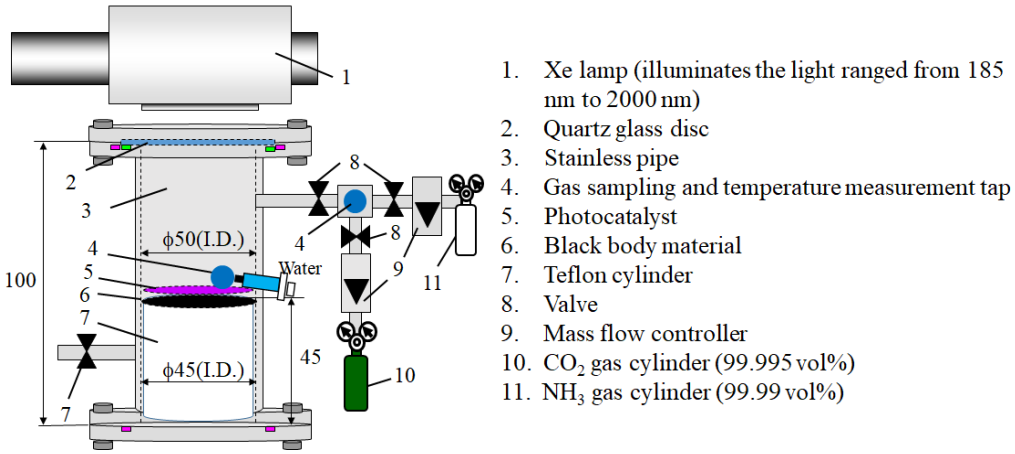

Figure 6. Schematic diagram of CO_2 reduction experimental apparatus. The reactor consists of stainless pipe, TiO_2 film photocatalyst positioned on Teflon cylinder, a quartz grass disc, a 150 W Xe lamp, mass flow controller, CO_2 gas cylinder, and NH_3 gas cylinder.

After filling the CO_2 gas with a purity of 99.995 vol% and NH_3 with a purity of 99.99 vol%, they are controlled by a mass controller and introduced into the reactor pre-vacuumed by a vacuum pump for 15 min. The valves are then installed at the inlet and the outlet of the reactor was closed during CO_2 reduction with NH_3. After that, this study confirmed the pressure of 0.1 MPa and gas temperature at 298 K in the reactor. Due to the heat of IR light components illuminated by the Xe lamp, the temperature of the gas in the reactor rose. The temperature of the experimental room was controlled and set at 293 K by an air conditioner. The molar ratio of CO_2/NH_3 was changed by 1:0.5, 1:1, 1:2, 1:4, 3:2, and 3:8. The reacted gas filled in the reactor was extracted by gas syringe via a gas sampling tap and it was analyzed by an FID gas chromatograph (GC353B, produced by GL Science) and a methanizer (MT221, produced by GL Science). The FID gas chromatograph and methanizer have a minimum resolution of 1 ppmV. The temperature of the gas in the reactor was measured by a thermocouple installed in the tap, which was located 1 mm above the TiO_2 film coated on a netlike glass disc. The CO_2 reduction experiment was conducted for up to 8 h. Gas sampling and temperature measurements were carried out from the start of the experiment until 8 h by 2 h.

4. Conclusions

From the investigation in this study, the following conclusions are drawn:

(i) The mismatch between the theoretical molar ratio to produce CO and the optimum molar ratio obtained with W/O B.B. as well as W B.B.-1 is confirmed. As the products near the photocatalyst surface might remain, the photocatalytic CO_2 reduction perfor-

mance is smaller under the investigated conditions with W/O B.B. and W B.B.-1 in this study.

(ii) The highest concentration of formed CO occurring in the case of CO_2:NH_3 = 3:2 with W B.B.-3 is higher than that with W B.B.-1 by 175 ppmV. It is revealed that the impact of the natural thermosiphon movement of gasses around the TiO_2 photocatalyst created by black body material on CO_2 reduction performance is larger with W B.B.-3.

(iii) There is almost no difference between the W B.B.-1 case and the W/O B.B. case in terms of gas temperature and the maximum concentration of formed CO.

(iv) The temperature of the gas in the reactor with W B.B.-3 is approximately 10 °C higher than that with W/O B.B. The maximum concentration of formed CO with W B.B.-3 is two to five times as large as that with W/O B.B.

(v) Comparing the heat capacity of black body material with that of the mixed gas of CO_2 and NH_3, it is revealed that one black body material is not enough to heat the mixed gas of CO_2 and NH_3 in the reactor. Three black body materials are needed to heat up the mixed gas of CO_2 and NH_3 in the reactor.

Author Contributions: Conceptualization and writing—original draft preparation, A.N.; data curation, T.K.; methodology, H.M.; writing—review and editing, E.H. All authors have read and agreed to the published version of the manuscript.

Funding: This research was funded by Mie University and JSPS KAKENHI Grant Number JP21K04769.

Acknowledgments: The authors acknowledge JSPS KAKENHI Grant Number JP21K04769.

Conflicts of Interest: The authors declare no conflict of interest.

References

1. Global Monitoring Laboratory. Available online: https://www.esrl.noaa.gov/gmd/ccgg/trends/global.html (accessed on 8 March 2022).
2. Jesic, D.; Jurkovic, L.D.; Pohar, A.; Suhadolnik, L.; Likozar, B. Engineering Photocatalytic and Photoelectrocatalytic CO_2 Reduction Reactions: Mechanisms, Intrinsic Kinetics, Mass Transfer Resistances, Reactors and Multi-scale Modeling Simulations. *Chem. Eng. J.* **2021**, *407*, 126799. [CrossRef]
3. Razzaq, A.; Ali, S.; Asif, M.; In, S.I. Layered Double Hydroxide (LDH) Based Photocatalysts: An Outstanding Strategy for Efficient Photocatalytic CO_2 Reduction. *Catalysts* **2020**, *10*, 1185. [CrossRef]
4. Matavos-Aramyan, S.; Soukhakian, S.; Jazebizadeh, M.H.; Moussavi, M.; Hojjati, M.R. On Engineering Strategies for Photoselective CO_2 Reduction—A through Review. *Appl. Mater. Today* **2020**, *18*, 100499. [CrossRef]
5. Remiro-Buenamanana, S.; Garcia, H. Photoassisted CO_2 Conversion into Fuels. *Chem. Cat Chem. Minirev.* **2019**, *11*, 342–356.
6. Zhu, S.; Chen, X.; Li, Z.; Ye, X.; Liu, Y.; Chen, Y.; Yang, L.; Chen, M.; Zhang, D.; Li, G.; et al. Cooperation between Inside and Outside of TiO_2: Lattice Cu^+ Accelerates Carrier Migration to the Surface of Metal Copper for Photocatalytic CO_2 Reduction. *Appl. Catal. B Environ.* **2020**, *264*, 118515. [CrossRef]
7. She, H.; Zhao, Z.; Bai, W.; Huang, J.; Wang, L.; Wang, Q. Enhanced Performance of Photocatalytic CO_2 Reduction via Synergetic Effect between Chitosan and Cu: TiO_2. *Mater. Res. Bull.* **2020**, *124*, 110758. [CrossRef]
8. Chen, X.; Ye, X.; He, J.; Pan, L.; Xu, S.; Xiong, C. Preparation of Fe^{3+}-doped TiO_2 Aerogels for Photocatalytic Reduction of CO_2 to Methanol. *J. Sol.-Gel. Sci. Technol.* **2020**, *95*, 353–359. [CrossRef]
9. Su, K.Y.; Chen, C.Y.; Wu, R.J. Preparation of Pd/TiO_2 Nanowires for the Photoreduction of CO_2 into Renewable Hydrocarbon Fuels. *J. Taiwan Inst. Chem. Eng.* **2019**, *96*, 409–418. [CrossRef]
10. Camarillo, R.; Toston, S.; Martinez, F.; Jimenez, C.; Rincon, J. Enhancing the Photocatalytic Reduction of CO_2 through Engineering of Catalysts with High Pressure Technology: Pd/TiO_2 Photocatalysts. *J. Supercrit. Fluids* **2017**, *123*, 18–27. [CrossRef]
11. Wei, Y.; Wu, X.; Zhao, Y.; Wang, L.; Zhao, Z.; Huang, X.; Liu, J.; Li, J. Efficient Photocatalyst of TiO_2 Nanocrystal-supported PtRu Alloy Nanoparticles for CO_2 Reduction with H_2O: Synergistic Effect of Pt-Ru. *Appl. Catal. B Environ.* **2018**, *236*, 445–457. [CrossRef]
12. Zhao, Y.; Wei, Y.; Wu, X.; Zheng, H.; Zhao, Z.; Liu, J.; Li, J. Graphene-wrapped Pt/TiO_2 Photocatalysts with Enhanced Photogenerated Charges Separation and Reactant Adsorption for High Selective Photoreduction of CO_2 to CH_4. *Appl. Catal. B Environ.* **2018**, *226*, 360–372. [CrossRef]
13. Toston, S.; Camarillo, R.; Martinez, F.; Jimenez, C.; Rincon, J. Supercritical Synthesis of Platinum-modified Titanium Dioxide for Solar Fuel Production from Carbon Dioxide. *Chin. J. Catal.* **2017**, *38*, 636–650. [CrossRef]
14. Jiang, Z.; Zhang, X.; Yuan, Z.; Chen, J.; Huang, B.; Dionysios, D.D.; Yang, G. Enhanced Photocatalytic CO_2 Reduction via the Synergistic Effect between Ag and Activated Carbon in TiO_2/AC-Ag Ternary Composite. *Chem. Eng. J.* **2018**, *348*, 592–598. [CrossRef]

15. Jiao, J.; Wei, Y.; Zhao, Y.; Zhao, Z.; Duan, A.; Liu, J.; Pang, Y.; Li, J.; Jiang, G.; Wang, Y. AuPd/3DOM-TiO_2 catalysts for photocatalytic reduction of CO_2: High efficient separation of photogenerated charge carriers. *Appl. Catal. B Environ.* **2017**, *209*, 228–239. [CrossRef]
16. Wang, L.; Zhu, B.; Cheng, B.; Zhang, J.; Zhang, L.; Yu, J. In-situ Preparation of TiO_2/N-doped Graphene Hollow Sphere Photocatalyst with Enhanced Photocatalytic CO_2 Reduction Performance. *Chin. J. Catal.* **2021**, *42*, 1648–1658. [CrossRef]
17. Wang, Z.W.; Wan, Q.; Shi, Y.Z.; Wang, H.; Kang, Y.Y.; Zhu, S.Y.; Liu, S.; Wu, L. Selective Photocatalytic Reduction CO_2 to CH_4 on Ultrathin TiO_2 Nanosheet via Coordination Activation. *Appl. Catal. B Environ.* **2021**, *288*, 120000. [CrossRef]
18. Pan, H.; Wang, X.; Xiong, Z.; Sun, M.; Muruganganthan, M.; Zhang, Y. Enhanced photocatalytic CO_2 reduction with defective TiO_2 nanotubes modified by single-atom binary metal components. *Environ. Res.* **2021**, *198*, 111176. [CrossRef]
19. Baniamer, M.; Aroujalian, A.; Sharifnia, S. Photocatalytic Membrane Reactor for Simultaneous Separation and Photoreduction of CO_2 to Methanol. *Int. J. Energy Res.* **2020**, *45*, 2353–2366. [CrossRef]
20. Molinari, R.; Lavorato, C.; Argurio, P. The Evolution of Photocatalytic Membrane Reactors over the Last 20 Years: A State of the Art Perspective. *Catalysts* **2021**, *11*, 775. [CrossRef]
21. Nishimura, A.; Komatsu, N.; Mitsui, G.; Hirota, M.; Hu, E. CO_2 Reforming into Fuel Using TiO_2 Photocatalyst and Gas Separation Membrane. *Catal. Today* **2009**, *148*, 341–349. [CrossRef]
22. Nishimura, A.; Sakakibara, Y.; Koshio, A.; Hu, E. The Impact of Amount of Cu on CO_2 Reduction Performance of Cu/TiO_2 with NH_3 and H_2O. *Catalysts* **2021**, *11*, 610. [CrossRef]
23. Nishimura, A.; Shimada, R.; Sakakibara, Y.; Koshio, A.; Hu, E. Comparison of CO_2 Reduction Performance with NH_3 and H_2O between Cu/TiO_2 and Pd/TiO_2. *Molecules* **2021**, *26*, 2904. [CrossRef] [PubMed]
24. Nahar, S.; Zain, M.F.M.; Kadhum, A.A.H.; Abu, H.H. Advances in Photocatalytic CO_2 Reduction with Water: A Review. *Materials* **2017**, *10*, 629. [CrossRef] [PubMed]
25. Tahir, M.; Amin, N.S. Advances in Visible Light Responsive Titanium Oxide Based Photocatalysts for CO_2 Conversion to Hydrocarbon Fuels. *Energy Convers. Manag.* **2013**, *76*, 194–214. [CrossRef]
26. Goren, Z.; Willner, I.; Nelson, A.J. Selective Photoreduction of CO_2/HCO_3^- to formate by aqueous suspensions and colloids of Pd-TiO_2. *J. Physic. Chem.* **1990**, *94*, 3784–3790. [CrossRef]
27. Tseng, I.H.; Chang, W.C.; Wu, J.C.S. Photoreduction of CO_2 Using Sol-gel Derived Titania and Titania-supported Copper Catalysts. *Appl. Catal. B* **2002**, *37*, 37–38. [CrossRef]
28. Izumi, Y. Recent Advances in the Photocatalytic Conversion of Carbon Dioxide to Fuels with Water and/or Hydrogen Using Solar Energy and Beyond. *Coord. Chem. Rev.* **2013**, *257*, 171–186. [CrossRef]
29. Lo, C.C.; Hung, C.H.; Yuan, C.S.; Wu, J.F. Photoreduction of Carbon Dioxide with H_2 and H_2O over TiO_2 and ZrO_2 in a Circulated Photocatalytic Reactor. *Sol. Energy Mater. Sci.* **2007**, *91*, 1765–1774. [CrossRef]
30. Nishimura, A.; Ishida, N.; Tatematsu, D.; Hirota, M.; Koshio, A.; Kokai, F.; Hu, E. Effect of Fe Loading Condition and Reductants on CO_2 Reduction Performance with Fe/TiO_2 Photocatalyst. *Int. J. Photoenergy* **2017**, *2017*, 1625274. [CrossRef]
31. Nishimura, A.; Sakakibara, Y.; Inoue, T.; Hirota, M.; Koshio, A.; Kokai, F.; Hu, E. Impact of Molar Ratio of NH_3 and H_2O on CO_2 Reduction Performance over Cu/TiO_2 Photocatalyst. *Phys. Astron. Int. J.* **2019**, *3*, 176–182.
32. Nemoto, J.; Goken, N.; Ueno, K. Photodecomposition of Ammonia to Dinitrogen and Dihydrogen on Platinized TiO_2 Nanoparticles in an Aqueous Solution. *J. Photochem. Photobiol. A Chem.* **2007**, *185*, 295–300. [CrossRef]
33. Japan Society of Mechanical Engineering. *Heat Transfer Hand Book*, 1st ed.; Maruzen: Tokyo, Japan, 1993; pp. 238, 367–369.
34. Abe, T.; Tanizawa, M.; Watanabe, K.; Taguchi, A. CO_2 Methanation Property of Ru Nanoparticle-loaded TiO_2 Prepared by a Polygonal Barrel-sputtering Method. *R. Soc. Chem.* **2009**, *2*, 315–321. [CrossRef]
35. Tahir, M.; Amin, N.S. Photocatalytic Reduction of Carbon Dioxide with Water Vapors over Montmorillonite Modified TiO_2 Nanocomposites. *Appl. Catal. B Environ.* **2013**, *142–143*, 512–522. [CrossRef]
36. Anzai, A.; Fukuo, N.; Yamamoto, A.; Yoshida, H. Highly Selective Photocatalytic Reduction of Carbon Dioxide with Water over Silver-loaded Calcium Titanate. *Catal. Commun.* **2017**, *100*, 134–138. [CrossRef]
37. CHINO. Available online: https://www.chino.co.jp/support/technique/thermometers_index/housyaritsu/ (accessed on 12 April 2022).
38. List for Physical Properties of Material. Available online: https://www.ohm.jp/media/tech_cooling204.pdf (accessed on 12 April 2022).
39. List for Physical Properties of Metal Element. Available online: https://www.nikkin-flux.co.jp/technology/up_img/1338425712-232811.pdf (accessed on 12 April 2022).